

# Controllable Fano-type optical response and four-wave mixing via magnetoelastic coupling in a opto-magnomechanical system

Amjad Sohail,<sup>1,\*</sup> Rizwan Ahmed,<sup>2</sup> Jia-Xin Peng,<sup>3,†</sup> Aamir Shahzad,<sup>1</sup>  
Tariq Munir,<sup>1</sup> S. K. Singh,<sup>4,‡</sup> and Marcos César de Oliveira<sup>5,§</sup>

<sup>1</sup>*Department of Physics, Government College University, Allama Iqbal Road, Faisalabad 38000, Pakistan.*

<sup>2</sup>*Physics division, Pakistan institute of nuclear science and technology (PINSTECH), Nilore, Islamabad 45650 Pakistan*

<sup>3</sup>*State Key Laboratory of Precision Spectroscopy, Quantum Institute for Light and Atoms,  
Department of Physics, East China Normal University, Shanghai 200062, People's Republic of China*

<sup>4</sup>*Graphene and Advanced 2D Materials Research Group (GAMRG),  
School of Engineering and Technology, Sunway University, No. 5,*

*Jalan Universiti, Bandar Sunway, 47500 Petaling Jaya, Selangor, Malaysia*

<sup>5</sup>*Instituto de Física Gleb Wataghin, Universidade Estadual de Campinas, Campinas, SP, Brazil*

We analytically investigate the Fano-type optical response and four-wave mixing (FWM) process by exploiting the magnetoelasticity of a ferromagnetic material. The deformation of the ferromagnetic material plays the role of mechanical displacement, which is simultaneously coupled to both optical and magnon modes. We report that the magnetostrictively induced displacement demonstrates Fano profiles, in the output field, which is well-tuned by adjusting the system parameters, like effective magnomechanical coupling, magnon detuning, and cavity detuning. It is found that the magnetoelastic interaction also gives rise to the FWM phenomenon. The number of the FWM signals mainly depends upon the effective magnomechanical coupling and the magnon detuning. Moreover, the FWM spectrum exhibits suppressive behavior upon increasing (decreasing) the magnon (cavity) decay rate. The present scheme will open new perspectives in highly sensitive detection and quantum information processing.

## I. INTRODUCTION

Cavity optomechanics is a rapidly growing area of theoretical and experimental research that explores the coherent coupling between mechanical and optical modes through the radiation pressure force of photons being trapped inside optomechanical cavities [1]. It has been responsible for significant advances in quantum technology, particularly when nonlinearities are available. We mention quantum information processing [2], quantum walk implementation [3], ultrahigh-precision measurement [4, 5], higher-order sidebands generation [6], optical nonlinearity [7], single photon blockade [8, 9], quantum entanglement [10–13], gravitation-wave detection [14, 15], optomechanically induced transparency (OMIT) [16–18], and optomechanically induced absorption (OMIA) [19] including optomechanically induced stochastic resonance [20]. In OMIT, analogously to electromagnetic induced transparency (EIT) [21], the radiation pressure-induced mechanical oscillations lead to destructive interference and hence significantly alter the optical response as well as its group delay [22, 23].

Another important and fascinating non-linear phenomenon is the interference and quantum coherence, called Fano resonance [24], where the prominent feature is a steep and sharp asymmetric line profile. Fano resonance were theoretically discovered by Ugo Fano [25], who found that the interaction of a discrete excited state of an atom with a continuum

of scattering states, is entirely different from the resonance phenomena delineated by the Lorentzian formula [25]. Fano interference has important applications such as in lasing without population inversion [26], as a probe to study decoherence [27], and as a way to improve the efficiency of heat engines [28]. Moreover, the radiating two coupled-resonators model, in which the two resonators have quite different lifetime can be used to explain the Fano line shapes [29, 30]. So the lifetimes of these modes are very significant in observing the Fano line shapes [31] and can be easily obtained in plasmonic systems [32] and metamaterial structures [33, 34]. Fano resonance has been recently studied in cavity magnomechanics [35] and magnon-qubit system [36].

Four-wave mixing (FWM), as the most engrossing nonlinear optical effect, is widely studied in optomechanical systems [37]. FWM is based on interference and quantum coherence and is extensively used to enlarge the frequency span of coherent light sources to ultraviolet and infrared [38, 39]. Multi-wave or FWM-mixing processes allow many vital physical processes, such as realizing optical bistability [40], normal mode splitting [41] or generating two coexisting pairs of narrowband biphotons [42]. Consequently, the FWM effect has gained much attention from researchers. Jiang et al. examined the controllability and tunability of the FWM process by driving the two cavities in a two-mode cavity optomechanical system at their respective red sidebands [43]. Wang and Chen studied the enhancement of the FWM response [44]. It must be pointed out that FWM is a weak phenomenon, which makes it hard to be realized in experiments. Therefore new directions are being proposed to improve the strength of those nonlinear phenomena.

The hybridization of different modes in cavity magnomechanics (CMM) opens up a promising platform to explore numerous non-linear quantum effects [45]. Magnome-

\*Electronic address: [amjadsohail@gcuf.edu.pk](mailto:amjadsohail@gcuf.edu.pk)

†Electronic address: [18217696127@163.com](mailto:18217696127@163.com)

‡Electronic address: [singhshailendra3@gmail.com](mailto:singhshailendra3@gmail.com)

§Electronic address: [marcos@ifi.unicamp.br](mailto:marcos@ifi.unicamp.br)

chanical systems consider a geometry such that an optical mode directly (indirectly) couples with a magnon mode (mechanical mode). They are based totally on magnons-quanta of spin waves in Ferrimagnetic materials [46], such as yttrium iron garnet (YIG), which provide a versatile and new platform to investigate strong light-matter interactions [47]. Strong interactions are due to two main reasons: (1) The Spin density of the YIG material is very high; (2) The damping rate of the YIG material is very low. Therefore, in the last decade, CMM has been explored in theoretical as well as an experimental domain because of its potential applications for observing macroscopic quantum states [48], quantum sensing [49] and magnomechanically induced transparency (MMIT) [35, 50, 51]. In CMM systems, the microwave (MW) cavity field is coupled to a magnon mode in a ferromagnetic YIG sphere [11] as well as the magnon mode also couples to a (vibrational) mechanical mode of the sphere through the magnetostrictive force [52]. Such magnomechanical interaction is dispersive [45, 53] in a similar fashion to radiation pressure interaction, leading to several theoretical and experimental investigations to study various quantum phenomena in cavity magnomechanical systems analogous to cavity optomechanics, such as magnomechanically induced transparency (MMIT) [35, 45], magnetically tunable slow light [51, 54], exceptional points [55], tripartite magnon-photon-phonon entanglement and Einstein-Podolsky-Rosen steerable nonlocality [56], cooling of mechanical motion [57], phonon lasing [58] and parity-time-related phenomena [59].

In this paper, we propose an unconventional and advantageous opto-magnomechanical system (OMMS) setup which is a composite architecture based on the indirect coupling of optical photons and magnon modes via the phononic mode (vibrational mode of the magnon) as shown in Fig. 1(a). The magnetoelastic coupling is responsible for the geometric deformation of the magnon in a YIG bridge which forms the vibrational motion. We consider that the phonon frequency is much smaller than the frequency of the magnon and in this situation, the dispersive interaction between the phonon and magnon modes becomes dominant (See Appendix A for details). This present scheme can be well fabricated by placing a high reflectivity small size mirror on the surface (edge) of the YIG bridge and therefore, the vibrational motion of the magnon can be easily coupled to an optical cavity through the radiation pressure, assembling an optomechanical cavity. However, the tiny size of the mirror does not affect the vibrations of the YIG bridge. In addition, such kind of indirect coupling between optical photons and magnons can easily be realized by assuming the low mechanical damping rate  $\gamma_b$  both in the optomechanical and magnomechanical cooperativities  $C_{om} = \frac{G_c^2}{\kappa_c \gamma_b} > 1$  ( $\kappa_c$  being the cavity decay rate), and  $C_{mm} = \frac{G_m^2}{\kappa_m \gamma_b} > 1$  ( $\kappa_m$  being the magnon decay rate) respectively, under present-day technology [1, 45, 60]. Moreover, experimentally feasible parameters have been taken for the current scheme. In this paper, we have presented several interesting results for generating/controlling Fano profiles and the FWM by varying many system parameters.

The current article is arranged as follows. In Sect. 2, we

present the theoretical model and the corresponding Hamiltonian of the OMMS. Section 3 designates the dynamics of the OMMS by exploiting the standard quantum Langevin approach, to get the expression for the optical response and the FWM process. In Sect. 4, we analytically discuss the optical response and the FWM process in detail. Finally, the conclusion is given in the last Sect. 5.

## II. THE MODEL AND THE DYNAMICS

The opto-magnomechanical system under consideration consists of an optical mode  $c$  and a slab of YIG nanoresonator in which collective excitation of a number of spins are coupled to mechanical vibrations [46]. It is vital to mention here that a micrometer size YIG bridge can well support a gigahertz (megahertz) magnon mode (vibrational mode) [46]. Therefore, such a magnomechanical system has a strong magnon-phonon dispersive coupling [61–63]. The present scheme can be accomplished by placing a small mirror on the edge (surface) of the YIG bridge as shown in Fig. 1 (a), and in this way, an optical field can be coupled to the magnetostriction-induced mechanical displacement via radiation pressure force. The fabricated mirror should be highly refractive, light, and small such that it will not affect the mechanical properties of the ferrimagnet. Therefore, in this way the magnomechanical displacement can be probed by light exploiting the optomechanical interaction, which is further used to determine the magnon population [64]. Moreover, the deformation mode (displacement of the mechanical resonator) is along the direction of the sticky surface area of the slab, such that the tightly coupled YIG bridge and the mirror resonate with the same frequency. In addition, the dispersive magnetostrictive interaction between magnon and phonon modes depends on the resonance frequencies of these coupled modes [65].

It is important to mention here that Fig.1 is only a diagrammatic sketch of one of the possible configurations to couple the magnomechanically induced displacement to an optical cavity. In addition, one doesn't have to attach a mirror (on the surface of the microbridge) to form the optical cavity. Alternatively, one can also adopt the analogy of taking a "membrane-in-the-middle" configuration by positioning the YIG sample inside the optical cavity. In this setup, the magnomechanically induced displacement can also be dispersively coupled to the optical cavity. In this case, no additional damping of the mechanical mode is needed. In the current study, we consider a large size crystal such that the magnon frequency is considered to be much greater than the vibrational frequency of the phononic mode such that the dispersive interaction between magnon and phonon modes, becomes dominant [45, 66]. The Hamiltonian of the present OMMS reads

$$H/\hbar = H_o + H_{in} + H_{dr}, \quad (1)$$

where

$$H_o = \omega_c c^\dagger c + \omega_m m^\dagger m + \frac{\omega_b}{2}(q^2 + p^2), \quad (2)$$

$$H_{in} = g_{mb} m^\dagger m q - g_{cb} c^\dagger c q, \quad (3)$$

$$H_{dr} = i\Omega(m^\dagger e^{-i\omega_o t} - m e^{i\omega_o t}) + i \sum_{f=L,p} \varepsilon_f (c^\dagger e^{-i\omega_f t} - c e^{i\omega_f t}). \quad (4)$$

where  $c(m)$  and  $c^\dagger (m^\dagger)$  are the respective annihilation and creation operators for the cavity (magnon) mode.  $p$  and  $q$  are the dimensionless momentum and position of the phononic mode (deformation vibrational mode), considered as a mechanical resonator, which simultaneously couples to the cavity (magnon) mode via radiation pressure interaction  $g_{cb}$  (dispersive magnetostrictive interaction  $g_{mb}$ ). The details of the optomechanical coupling  $g_{cb}$  can be seen in [67] while the detailed discussion about the magnomechanical coupling  $g_{mb}$  is present in Appendix A. In addition,  $\omega_c(\omega_m)[\omega_b]$  is the resonance frequencies of the cavity mode (magnon mode) [phononic mode].  $\omega_m$  can be flexibly tuned via  $\omega_m = \gamma_0 H_m$ , where  $H_m$  is the bias magnetic field and  $\gamma_0$  is the gyromagnetic ratio. The Rabi frequency  $\Omega = (\sqrt{5}/4) \gamma_0 \sqrt{N_s} B_0$  [48] represents the coupling strength of the input laser drive field with frequency  $\omega_0$ , where  $\gamma_0 = 28\text{GHz/T}$ ,  $B_0 = 3.9 \times 10^{-9}\text{T}$  and the total number of spins  $N_s = \rho V$ , where  $\rho = 4.22 \times 10^{27}\text{m}^{-3}$  denotes the spin density and  $V$  being the volume of

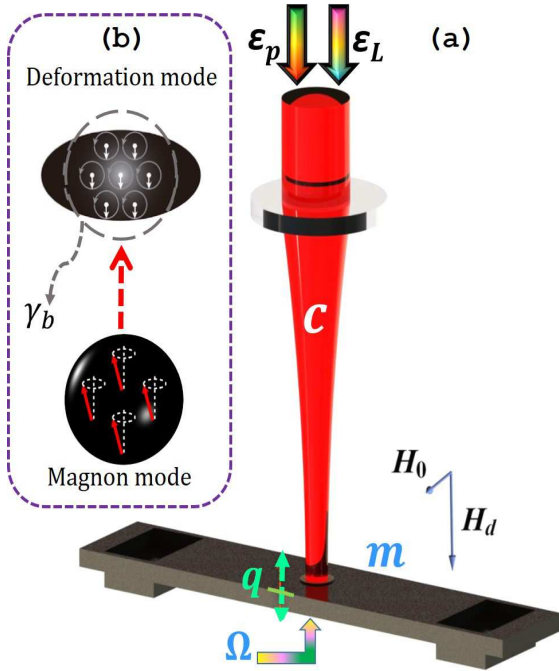


FIG. 1: (Color Online) (a) Schematic diagram of the optomagnomechanical system where mechanical displacement is simultaneously coupled to the magnonic mode via the dispersive magnetostrictive interaction and to an optical cavity through radiation pressure force. (b) Schematic diagram of the Kittel and deformation modes.

the YIG bridge. In addition, we apply the Holstein-Primakoff transformation to the bosonic operators for the magnon ( $m$  and  $m^\dagger$ ), which basically form from the collective motion of the spins. In fact,  $\Omega$  can be derived by the basic low-lying excitations assumption i.e.,  $\langle m^\dagger m \rangle \ll 2N_s$ , where  $N$  ( $s = \frac{5}{2}$ ) is the total number of spin states (the spin number of the ground state  $\text{Fe}^{3+}$  ion) in YIG [68]. Furthermore, we also drive the optical cavity through external laser field with amplitude  $\varepsilon_L = \sqrt{\kappa_c \wp_L / \hbar \omega_L}$ , where  $\kappa_c$  is the decay rate of the optical cavity mode,  $\omega_L$  ( $\wp_L$ ) is the frequency (power) of the external input laser field. At the same time, the cavity mode is also driven by a weak probe field with amplitude  $\varepsilon_L$  and frequency  $\wp_p$ . The corresponding Hamiltonian of the OMMS, after the rotating wave approximation at the coupling frequency  $\omega_L$ , is given by

$$H/\hbar = \Delta_c^0 c^\dagger c + \Delta_m^0 m^\dagger m + \frac{\omega_b}{2}(q^2 + p^2) + g_{mb} m^\dagger m q - g_{cb} c^\dagger c q + i\Omega(m^\dagger - m) + i\varepsilon_L(c^\dagger - c) + i\varepsilon_p(c^\dagger e^{-i\delta t} - c e^{i\delta t}), \quad (5)$$

where  $\Delta_m^0 = \omega_m - \omega_L$ ,  $\Delta_c^0 = \omega_c - \omega_L$  and  $\delta = \omega_p - \omega_L$ .

Now, we discuss the dynamics of this OMMS by writing the corresponding QLEs, which are given by

$$\begin{aligned} \dot{q} &= \omega_b p, \\ \dot{p} &= \omega_b q - \gamma_b p - g_{mb} m^\dagger m + g_{cb} c^\dagger c + \xi, \\ \dot{c} &= -(i\Delta_c^0 + \kappa_c)c + ig_{cb} c q + \varepsilon_L + \varepsilon_p e^{-i\delta t} + \sqrt{\kappa_c} c^{in}, \\ \dot{m} &= -(i\Delta_m^0 + \kappa_m)m - ig_{mb} m q + \Omega + \sqrt{\kappa_m} m^{in}, \end{aligned} \quad (6)$$

where  $\kappa_c(\kappa_m)$  is the decay rate of the cavity mode (magnon mode), and  $\gamma_b$  is the damping rate of the vibrational mode. Furthermore,  $\xi$ ,  $c^{in}$  and  $m^{in}$  are, respectively, the input noise operators for the vibrational mode, cavity modes and magnon mode. The above QLEs can be linearized by writing  $z = z_s + \delta z$ , ( $z = p, q, c, m$ ), where  $z_s$  ( $\delta z$ ) is the steady state value (fluctuation) of any operator. For a sufficiently large amplitude of magnon and cavity modes, average value should be much greater than the fluctuation. Substituting the above ansatz into Eq.(6) and ignoring the higher order perturbations, the average values of the dynamical operators are given by

$$\begin{aligned} p_s &= 0, \\ q_s &= g_{cb} \frac{|c_s|^2}{\omega_b} - g_{cb} \frac{|m_s|^2}{\omega_b}, \\ c_s &= \frac{\varepsilon_L}{(i\Delta_c + \kappa_c)}, \\ m_s &= \frac{\Omega}{(i\Delta_m + \kappa_m)}, \end{aligned} \quad (7)$$

where  $\Delta_c = \Delta_c^0 - g_{cb} q_s$  and  $\Delta_m = \Delta_m^0 + g_{mb} q_s$  are the effective cavity and magnon mode detunings, respectively, which include the slight shift of frequency. The corresponding linearized QLEs, after ignoring quantum and thermal noise terms, are:

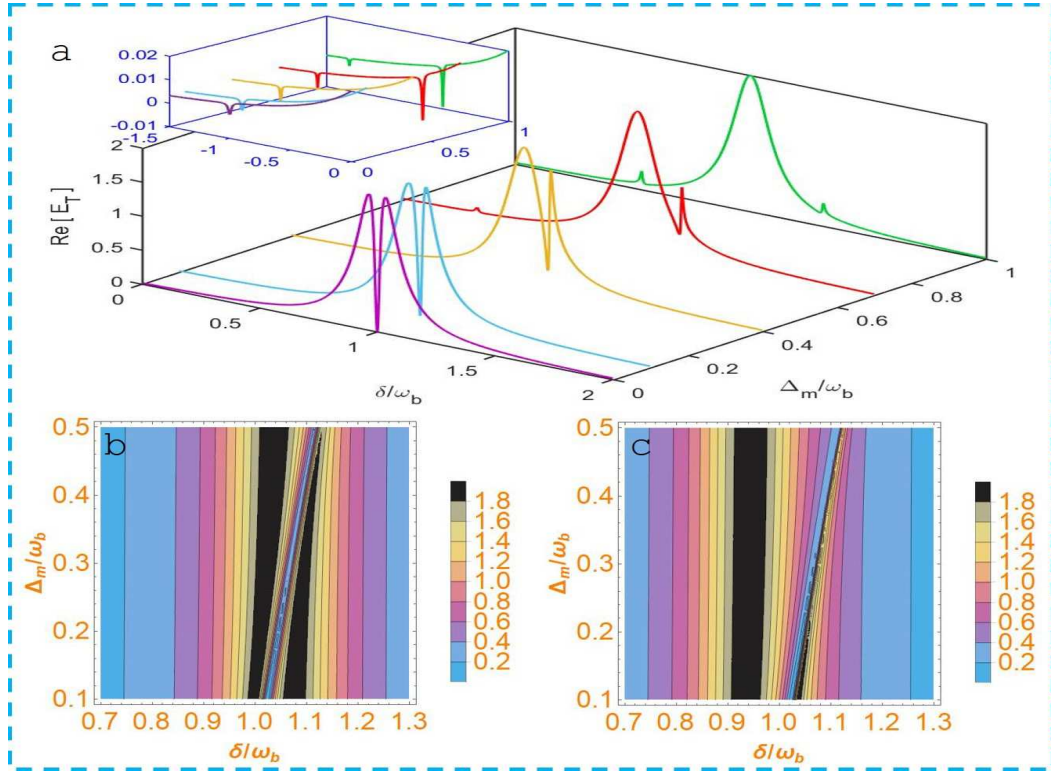


FIG. 2: (Color Online) (A) The real part  $\text{Re}(\epsilon_T)$  as a function of  $\delta/\omega_b$  and  $\Delta_m/\omega_b$  when  $\Delta_c/\omega_b = 1$ . Contour plot of real part  $\text{Re}(\epsilon_T)$  as a function of  $\delta/\omega_b$  and  $\Delta_m/\omega_b$  when (B)  $\Delta_c = 1.05\omega_b$  and (C)  $\Delta_c = 0.95\omega_b$ . The rest of the parameters are same as in Table .1.

$$\begin{aligned}
 \delta\dot{q} &= \omega_b\delta p, \\
 \delta\dot{p} &= \omega_b\delta q - \gamma_b\delta p - G_m\delta m^\dagger - G_m^*\delta m + G_c\delta c^\dagger + G_c^*\delta c, \\
 \delta\dot{c} &= -(i\Delta_c + \kappa_c)\delta c + iG_c\delta q + \varepsilon_p e^{-i\delta t}, \\
 \delta\dot{m} &= -(i\Delta_m + \kappa_m)\delta m - iG_m\delta q.
 \end{aligned} \tag{8}$$

Here,  $G_{mb} = \sqrt{2}g_{mb}m_s$  and  $G_{cb} = \sqrt{2}g_{cb}c_s$  are the effective magnomechanical and optomechanical coupling, respectively. The obtained fluctuation operators can then be solved by setting:  $\delta z = z_- e^{-i\delta t} + z_+ e^{i\delta t}$  where  $z_-$  and  $z_+$  (with  $z = q, p, c, m$ ) are much smaller than  $z_s$ . It is noteworthy to mention that the fluctuation operators contain many Fourier components after expansion. Moreover, the high-order terms can safely be neglected in the limit of weak signal field. Substituting the above ansatz into Eq. (8) and taking the lowest order in  $\varepsilon_p$ , we establish the final solution for the coefficients of optical response and FWM process as

$$c_- = \frac{[\omega_b^2 - \delta^2 - i\Theta_n]\varepsilon_p}{[\omega_b^2 - \delta^2 - i\Theta_n]\Omega_2^c - i\omega_b G_{cb}^2}, \tag{9}$$

and

$$c_+ = \frac{iG_{cb}^2\omega_b\Theta_p\varepsilon_p}{[\omega_b^2 - \delta^2 + i\Theta_p](\Omega_1^c)^* - i\omega_b G_{cb}^2}, \tag{10}$$

where

$$\begin{aligned}
 \Theta_n &= \delta\gamma_b - \omega_b\chi_{12}, & \Theta_p &= \delta\gamma_b + \omega_b\alpha_{12}, \\
 \chi_{12} &= G_{mb}^2\chi_1 + G_{cb}^2\chi_2, & \chi_1 &= [\Omega_2^m - \Omega_1^m][\Omega_1^m\Omega_2^m]^{-1}, \\
 \chi_2 &= [\Omega_1^c]^{-1}, & \alpha_2 &= [(\Omega_2^c)^*]^{-1}, \\
 \alpha_{12} &= G_{mb}^2\alpha_1 + G_{ab}^2\alpha_2, \\
 \alpha_1 &= [(\Omega_1^m)^* - (\Omega_2^m)^*][(\Omega_1^m)^*(\Omega_2^m)^*]^{-1}, \\
 \Omega_1^m &= \kappa_m - i(\Delta_m + \delta), & \Omega_2^m &= \kappa_m + i(\Delta_m - \delta), \\
 \Omega_1^c &= \kappa_c - i(\Delta_c + \delta), & \Omega_2^c &= \kappa_c + i(\Delta_c - \delta).
 \end{aligned}$$

### III. OUTPUT FIELD OF OMMS

To investigate the optical properties of the output field and the FWM process in OMMS, we start with the following standard input-output relation [69]

$$c_{out}(t) = c_{in}(t) - \sqrt{2\kappa_c}c(t). \tag{11}$$

In the above formula,  $c_{in}$  and  $c_{out}$  are, respectively the input field and output field operators. Furthermore, the expectation



value of the output field is given by

$$\begin{aligned}
c_{out}(t) &= \left( \sqrt{2\kappa_c}c_0 - \frac{\varepsilon_L}{\sqrt{2\kappa_c}} \right) e^{-i\omega_L t} \\
&+ \left( \sqrt{2\kappa_c}c_- - \frac{\varepsilon_p}{\sqrt{2\kappa_c}} \right) e^{-i(\delta+\omega_L)t} \\
&+ \sqrt{2\kappa_c}c_+ e^{i(\delta-\omega_L)t}, \\
&= \left( \sqrt{2\kappa_c}c_0 - \frac{\varepsilon_L}{\sqrt{2\kappa_c}} \right) e^{-i\omega_L t} \\
&+ \left( \sqrt{2\kappa_c}c_- - \frac{\varepsilon_p}{\sqrt{2\kappa_c}} \right) e^{-i\omega_p t} \\
&+ \sqrt{2\kappa_c}c_+ e^{i(\omega_p-2\omega_L)t}, \tag{12}
\end{aligned}$$

where the second (third) term corresponds to the components at the frequencies  $\omega_p$  ( $2\omega_L - \omega_p$ ) representing the optical (FWM) response of the system induced by the anti-Stokes (Stokes) scattering process. In addition,  $c_{out}(t)$  can also be expanded as

$$\begin{aligned}
\langle c_{out}(t) \rangle &= c_{out,0} e^{-i\omega_L t} + c_{out,-} e^{-i(\delta+\omega_L)t} \\
&+ c_{out,+} e^{i(\delta-\omega_L)t}, \tag{13}
\end{aligned}$$

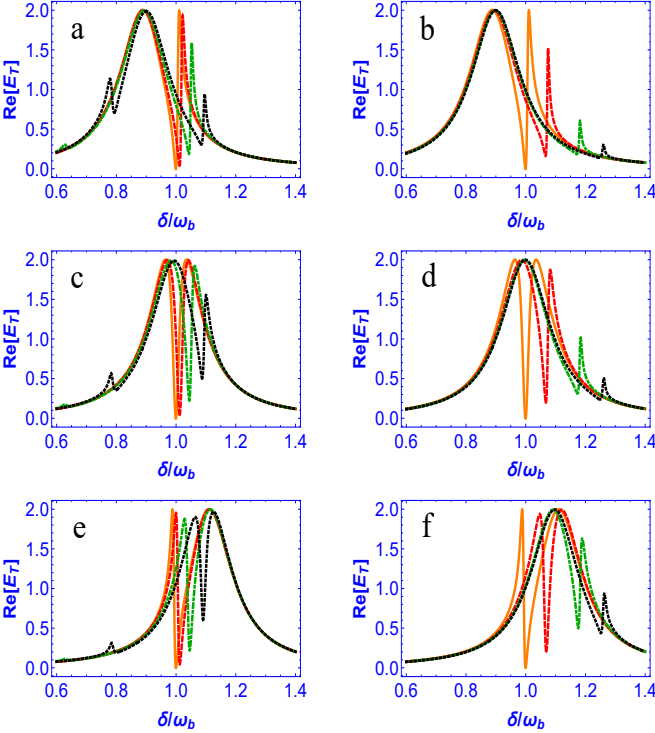


FIG. 3: (Color Online) The real part  $\text{Re}(\varepsilon_T)$  as a function of normalized detuning for different value of  $\Delta_m$  and  $G_{mb}$ . In figure(a-f), solid orange represents  $\Delta_m = 0$ , dashed red represents  $\Delta_m = 0.3\omega_b$ , dot-dashed green represents  $\Delta_m = 0.7\omega_b$  and solid gray represents  $\Delta_m = 0.9\omega_b$ . We take  $G_{mb} = 0.2\omega_b$  for the left panel and  $G_{mb} = 0.5\omega_b$  for the right panel. Moreover, we take  $\Delta_c = 0.9\omega_b$  in (a-b),  $\Delta_c = \omega_b$  in (c-d),  $\Delta_c = 1.1\omega_b$  in (e-f). The rest of the parameters are same as in Table .1.

Parameters	Symbol	Value
Decay rate of the cavity mode	$\kappa_c$	$0.1\omega_b$
Decay rate of the magnon mode	$\kappa_m$	$\simeq 0.1\kappa_c$
Mechanical damping rate	$\gamma_b$	$10^{-5}\omega_b$
Effective Cavity coupling	$G_{cb}$	$0.05\omega_b$
Effective magnon coupling	$G_{mb}$	$0.5\omega_b$

TABLE I: The parameters used in our calculations, taken from recent the experiments in Ref [45, 61, 71].

Comparing Eq. (12) and Eq. (13), we easily arrive at

$$\begin{aligned}
c_{out,-} &= \sqrt{2\kappa_c}c_- - \frac{\varepsilon_p}{\sqrt{2\kappa_c}}, \\
c_{out,+} &= \sqrt{2\kappa_c}c_+. \tag{14}
\end{aligned}$$

Finally, we obtain the following total output field relation at the probing frequency  $\omega_p$

$$\varepsilon_T = \frac{\sqrt{2\kappa_c}c_{out,-} + \varepsilon_p}{\varepsilon_p} = \frac{2\kappa_c c_-}{\varepsilon_p} = \Lambda + i\tilde{\Lambda}, \tag{15}$$

where  $\Lambda = \text{Re}[\varepsilon_T]$  and  $\tilde{\Lambda} = \text{Im}[\varepsilon_T]$  are, respectively, represent the in-phase and out-of-phase quadratures of the output probe field. In addition, one can obtained the absorptive (dispersive) behavior of the output probe field from  $\Lambda(\tilde{\Lambda})$  [70].

Similarly, at Stokes scattering, the FWM intensity can be obtained from output stokes field as

$$\varepsilon_{FWM} = \left| \frac{\sqrt{2\kappa_c}c_{out,+}}{\varepsilon_p} \right|^2 = \left| \frac{2\kappa_c c_+}{\varepsilon_p} \right|^2. \tag{16}$$

## IV. NUMERICAL RESULTS AND DISCUSSIONS

### A. Fano-type optical response

In this section, we present the frequency response and the FWM process in OMMS by employing the system parameters. For the present OMMS, we have selected parameters which are well experimentally realizable and are given in Table 1 [45, 61, 71]. The practical feasibility of these parameters is given in [71–73]. It is noteworthy that the cavity mode is weakly driven as compared to the driven magnon, leading to  $|c_s|^2 \ll |m_s|^2$  and therefore,  $G_{cb} \ll G_{mb}$ . Hence, one can safely claim that the megnetostrictive interaction is paramount over optomechanical interaction, i.e.,  $q_s \simeq -g_{cb} \frac{|m_s|^2}{\omega_b}$  (See Eq. (7)). In addition, it has already been proved that effective magnomechanical coupling,  $G_{mb}$  is almost 10 times greater than effective magnomechanical coupling,  $G_{cb}$  [64, 72]. Therefore for simplicity, we have assumed  $G_{mb} = (0.2 - 0.5)\omega_b$  and  $G_{cb} = 0.05\omega_b$ .

Fano resonances emerge due to the interaction between the cavity/magnon mode and the vibrational mode of the resonator. We have realized the resonances in the output spectra viz.  $\varepsilon_T = \Lambda + i\tilde{\Lambda}$ . Since OMIT originates by the constructive and destructive interference of different frequency

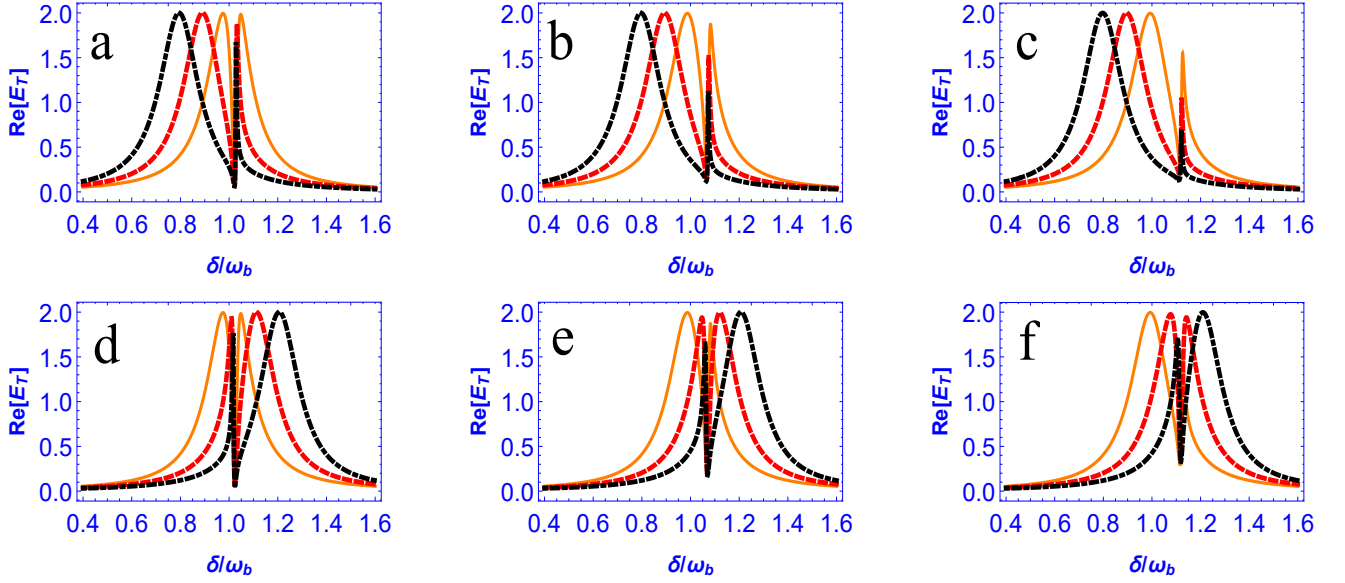


FIG. 4: (Color Online) The Real part  $\text{Re}(\varepsilon_T)$  as a function of normalized detuning for different value of  $\Delta_c$ . In figure(a-c), solid orange represents  $\Delta_c = \omega_b$ , dashed red represents  $\Delta_c = 0.9\omega_b$  and dot-dashed black represents  $\Delta_c = 0.8\omega_b$ . In figure(d-f), solid orange represents  $\Delta_c = \omega_b$ , dashed red represents  $\Delta_c = 1.1\omega_b$  and dot-dashed black represents  $\Delta_c = 1.2\omega_b$ . We take,  $\Delta_m = 0.1\omega_b$  in (a)(d),  $\Delta_m = 0.3\omega_b$  in (b)(e) and  $\Delta_m = 0.5\omega_b$  in (c)(f). The rest of the parameters are same as in Table .1.

contributions, it is well known that we can expect Fano profiles under some conditions [74]. We first note that when the magnon (or cavity) detuning is out of resonance with the vibrational frequency, for instance  $\Delta_m < \omega_b$  and  $\Delta_c \neq \omega_b$  (or even  $\Delta_c = \omega_b$ ), consequently Fano profiles emerge in OMIT spectra, in agreement with previous reports [18, 74]. To discuss the emergence and tunability of Fano profiles in OMMS, we first show the absorption spectra as a function of normalized detuning  $\delta/\omega_b$  for a fixed value of magnomechanical coupling rate  $G_{mb}$ , when  $\Delta_c = \omega_b$  in Fig. 2. Starting from  $\Delta_m/\omega_b = 0$ , we tuned the frequency  $\Delta_m$  in such a way that it approached the vicinity of the mechanical mode frequency  $\omega_b$  (see the green curve in Fig. 2 (a)). In the absence of magnon interaction, two dips in absorption can be found, which appear around  $\delta = \pm\omega_b$  as shown by the magenta line in Fig. 2 (a) (Also in inset). This is because in the present system, we have taken extremely low value of the damping rate and therefore the lowest value of the output field amplitude exist when  $\omega_b^2 - \delta^2 \simeq 0$  (or  $\delta = \pm\omega_b$ ). Consequently, we observe a typical OMIT windows around these points. However, the magnomechanical interaction involve to exhibit asymmetric Fano profiles as shown by the yellow, red and green lines in Fig. 2(a). In addition, we obtain a curve almost similar to Lorentzian when  $\Delta_m = \omega_b$ . Hence, the interaction of magnomechanical interaction leads to enhance the absorption around  $\delta = \omega_b$  around  $\Delta_m = \omega_b$ . However the peak of the Fano profiles gradually decrease with the increase of  $\Delta_m$ . The inset 3D figure in Fig. (a) exhibits the same absorption spectra in the blue-detuned region, which shows the small amplification of each curve occurs where we observe the dip in the red-detuned region. For example, the absorption dips (amplification dips) of the green line in red-detuned region occur at  $\delta = 0.55\omega_b$

( $\delta = -0.55\omega_b$ ) and  $\delta = 1.3\omega_b$  ( $\delta = -1.3\omega_b$ ) (-ve values can be seen in inset of Fig. 2(a)). To further shed light on the Fano profiles, we show the Fano profile spectra for a specific range of magnon detuning as density plots in Fig. 2 (b) and Fig. 2 (c) at  $\Delta_c = 1.05\omega_b$  and  $\Delta_c = 0.95\omega_b$  respectively. The Fano profiles become more prominent when we slightly shift the cavity detuning to higher frequency (see Fig. 2 (b)) as compared to the Fano profile spectra for the lower cavity detuned region (see Fig. 2 (c)).

As already discussed, the existence of Fano profiles in OMMS is due to the nonresonant interactions of magnon (or cavity) mode, the symmetry of the typical OMIT window is transfigured into asymmetric Fano profiles. Therefore, in the present OMMS, we investigate the Fano profile which can be tuned by the effective magnomechanical coupling strength  $G_{mb}$  and magnon detuning  $\Delta_m$  for both resonance ( $\Delta_c = \omega_b$ ) as well as a non-resonance case ( $\Delta_c \neq \omega_b$ ). In Fig. 3, we show a typical behavior of absorption spectra as a function of the normalized probe-coupling detuning for different values of  $\Delta_m$  and  $G_{mb}$ . We obtained a typical OMIT window in the absence of magnon interaction as show by the orange solid line in Fig. 3 (c-d). However, the asymmetry of the absorption spectra incenses with the increase of  $\Delta_m$  as shown by the dashed red, dot-dashed green and solid black lines. Similarly, Fig. 3 (a-b) shows the absorption spectra when  $\Delta_c = 0.9\omega_b$  and Fig. 3 (e-f) shows the absorption spectra when  $\Delta_c = 1.1\omega_b$ . The height of the Fano profiles decrease with the increase of  $\Delta_m$ . In addition, one can see that the width between the central absorption peak and sharp Fano profile for left panel of Fig. 3, is not prominently increase while for the right panel, it sufficiently increases. Therefore, it is clear from the above discussion, that  $\Delta_m$  ( $G_{mb}$ ) controls

the peak/dip (width) of the Fano profile.

In order to observe the combined effect of magnon and cavity detunings, we plot the absorption spectra by varying  $\Delta_m/\omega_b$  and  $\Delta_c/\omega_b$  in Fig. 4. We now present the absorption profile as a function of normalized detuning  $\delta/\omega_b$  at the fixed effective coupling strengths  $G_{mb}$  and  $G_{cb}$ . For a fixed value of  $\Delta_m/\omega_b$ , we continuously tuned the cavity detuning from  $\Delta_c = 0.8\omega_b$  to  $\Delta_c = 1.2\omega_b$  as shown in Fig. 4. It is noted that the Lorentzian type peak move left (right) as cavity detuning  $\Delta_c/\omega_b$  decreases (increases). However, the peak of the sharp Fano profile depends mainly on the magnon detuning  $\Delta_m/\omega_b$  i.e., peak (dip) decreases (move slightly upward) with the increase of  $\Delta_m/\omega_b$ .

### B. Four-wave mixing process

Compared with the typical cavity optomechanical system comprising a mechanical resonator coupled with an optical cavity via radiation pressure force, the OMMS under con-

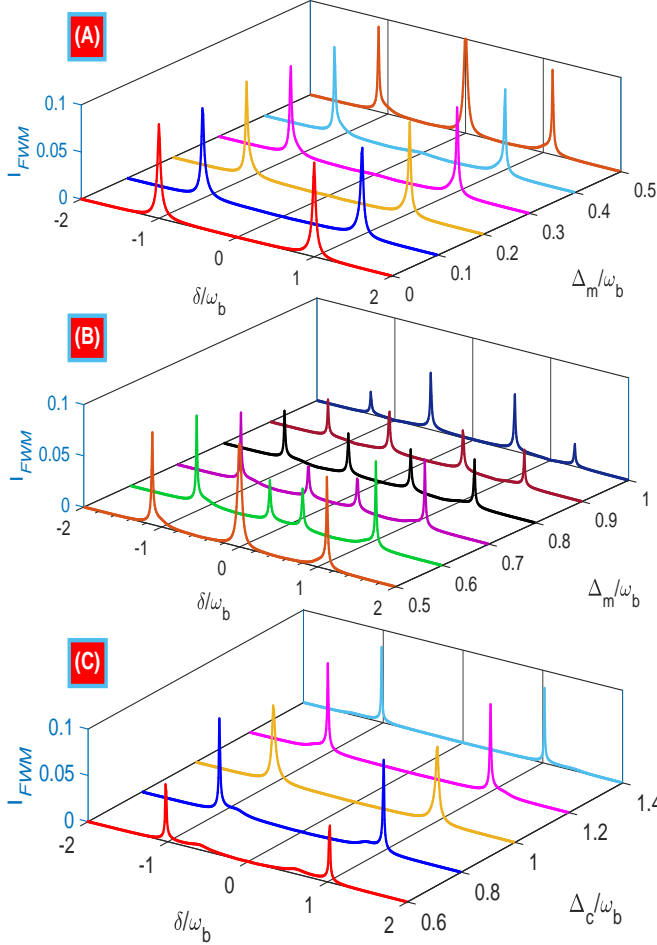


FIG. 5: (Color Online) FWM intensity  $I_{FWM}$  as a function of  $\delta/\omega_b$  and  $\Delta_m/\omega_b$ . We take  $\Delta_c = \omega_b$  in (a-b) and  $\Delta_m = 0.4\omega_b$  in (c). The rest of the parameters are same as in Table .1.

sideration allows a greater controllability on the FWM process. Here, we concentrate on different parameters to tune the FWM signals, i.e., the cavity/magnon detuning, the decay rate and effective magnomechanical coupling strength. Fig. 5(A) plots the FWM spectrum as a function of the pump-probe detuning for different values of the magnon detuning. It is shown in Fig. 5(A) that the two peaks of FWM signals are obtained exactly at  $\delta = \pm\omega_b$ , where OMMS exhibits transparency. The peaks at  $\delta = \pm\omega_b$  represent the intensity of the stokes field produced by the coupling field with the vibrational mode frequency. In addition, for  $\Delta_m < 0.4\omega_b$ , the FWM signal remains almost the same as shown in Fig. 5(A). However, one can see an extra peak located at  $\delta = 0$  along with the two peaks located at  $\delta \simeq \pm 0.1\omega_b$  appear when  $\Delta_m = 0.5\omega_b$ . Therefore, one can infer that the middle peak arises owing to the strong magnomechanical interaction. In addition, for  $\Delta_m \geq 0.6\omega_b$ , the peak at  $\delta = 0$  further split to create two peaks at  $\delta = \pm 0.2\omega_b$  along with two peaks at  $\delta = \pm 1.2\omega_b$ . However, the strength of the two peaks at  $\delta = \pm 0.2\omega_b$  sufficiently smaller than the two peaks around  $\delta = \pm\omega_b$ . It can be seen that as the magnomechanical interaction becomes strong (i.e., for  $\Delta_m \geq 0.6\omega_b$ ), the two peaks at  $\delta = \pm 0.2\omega_b$  become heighten as compared to the two peaks around  $\delta = \pm\omega_b$  as shown in Fig. 5(B). This effect becomes more prominent in Fig. 6(a-b). Furthermore, the width between the peaks gets broader by increasing  $\Delta_m$  as shown in Fig. 5(B). It is important to mention here that for increasing value of  $\Delta_m$ , the FWM signals at  $\delta = \omega_b$  ( $\delta = -\omega_b$ ) start moving to the right(left). Therefore, we infer that the signal at  $\delta = \pm\omega_b$  is completely

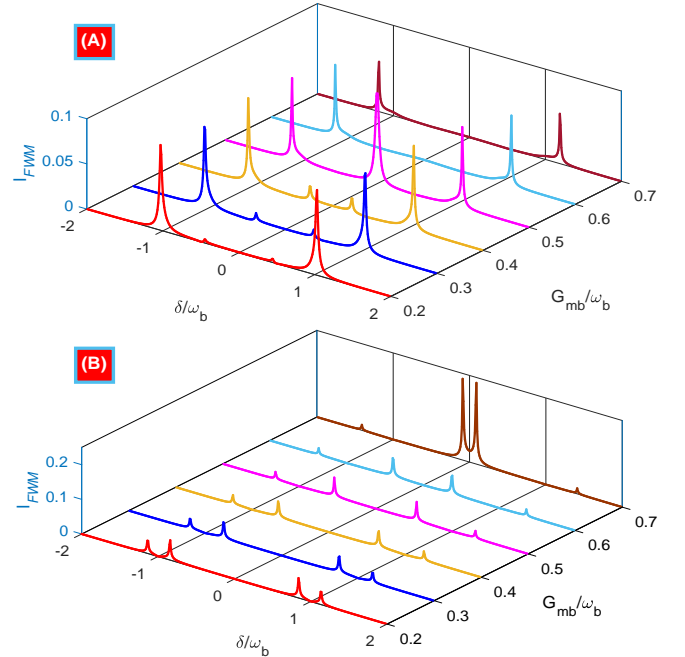


FIG. 6: (Color Online) FWM intensity  $I_{FWM}$  as a function of (A)  $\Delta_c/\omega_b$  and  $\delta/\omega_b$  and (B)  $G_{mb}/\omega_b$  and  $\delta/\omega_b$ . We take  $\Delta_m = 0.5\omega_b$  in (A) and  $\Delta_m = \omega_b$  in (B). The rest of the parameters are same as in Table .1.

suppressed at due to the destructive interference (see the dark blue line). Fig. 5(C) plots the FWM spectrum as a function of the pump-probe detuning for different value of the cavity detuning which clearly shows the FWM signal becomes strong as we increase  $\Delta_c$  and the width between the peaks remains constant.

Figure 6(A) shows the variation of the FWM spectrum as a function of the pump-probe detuning for different values of the effective magnon coupling strength  $G_{mb}$  when  $\Delta_m = 0.5\omega_b$ . It can be shown that the two less intensity middle peaks gets stronger and closer until  $G_{mb} \leq 0.4\omega_b$ . As the magnomechanical interaction becomes stronger, the two middle less intensified peaks then merged to form a single intensified peak for  $G_{mb} = 0.5\omega_b$ . Further enhancement of  $G_{mb}$  not only brings the peak at  $\delta = 0$  to an end but also decrease the intensity of two side peaks. Figure 6(B) shows the variation of the FWM spectrum as a function of the pump-probe detuning for different value of the effective magnon coupling strength  $G_{mb}$  when  $\Delta_m = \omega_b$ . One can observe that the two distant peaks move further apart while the two middle peaks come closer by increasing the value of the  $G_{mb}$ . In addition, the strength of the two distant peaks (middle peaks) decrease (increase) with the enhancement of  $G_{mb}$ . From the above discussion, one can easily conclude that the FWM signals can be tuned (enhanced) by varying different system's parameters.

The FWM process has been shown in cavity optomechanics, which strongly depends on the mean photon number. Varying the cavity decay rate  $\kappa_c$  (magnon decay rate  $\kappa_m$ ) will directly modify the mean photon number (magnon number). Therefore, we plot the FWM signal by varying the cavity and magnon decay rates. As shown in Fig. 7(A), the FWM signal is strong and the two peaks can be seen at  $\delta = \pm\omega_b$ . When the cavity decay rate is decreased, the two peaks of the FWM signal is sufficiently reduced. In addition, the two peaks located at  $\delta = \pm\omega_b$  transfigured to four diminished peaks located at  $\delta = \pm 0.95\omega_b$  and  $\delta = \pm 1.05\omega_b$ . Similarly, in Fig. 7(B), we investigate the influence of the magnon decay rate  $\kappa_m$  on the FWM intensity. Figure 7(B) shows that the FWM intensity is enhanced sufficiently with the increase of the magnon decay rate  $\kappa_m$ . Hence, one can infer that cavity and magnon decay rates have a substantial impact on the FWM process [44].

### C. Experimental Feasibility

In the following, we discuss the experimental feasibility of our proposed scheme. There exist two subsystems: (i) Magnomechanical part (ii) Optomechanical part. The adopted YIG micro-bridge (the magnomechanical subsystem) was based on the experimental demonstration [46]. However, the experimental demonstration of the optomechanical part has been demonstrated in many research papers [16, 17]. As for as experimental parameters are concerned, we have chosen parameters which are can easily be achieved using present-day technology. In addition, we have considered the parametric regime which is valid only when the magnon occupation number is significantly smaller than the total number of spin i.e.,  $m^\dagger m \ll 2N_s = 5N$ , where  $5N$  is the total

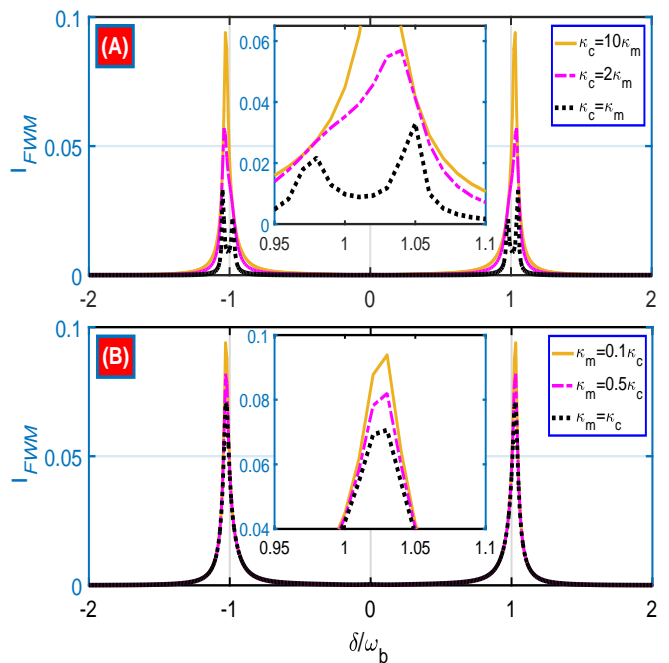


FIG. 7: (Color Online) FWM intensity  $I_{FWM}$  as a function of  $\delta/\omega_b$  for different values of (A)  $\kappa_c$  and (B)  $\kappa_m$ . We take  $\kappa_m = 0.01\omega_b$  in (A) and  $\kappa_c = 0.1\omega_b$  in (B). The rest of the parameters are same as in Table .1.

spin number of the  $Fe^{3+}$  ion in YIG  $s = 5/2$ . Our numerical results show that  $N$  is of the order of  $3.5 \times 10^{16}$  and  $\Omega = 712THz$  [45, 71]. It has been observed in the present study that these conditions are fulfilled and our scheme is feasible for strong magnon-phonon coupling. This is due to the strong magnon pump field, which causes unwanted nonlinear effects. However, as shown in recent experiments, a larger value of magnon-phonon coupling would result in a working regime, where we can drop the higher order terms due to a strongly driven magnomechanical system [71]. From the above discussion, we infer that we have chosen an experimentally feasible working regime. In near future, any experiment employing a planar cross-shaped cavity coupled to a magnon or can allow the implementation of the proposed scheme using a co-planar waveguide [77, 78].

### V. CONCLUSION

In conclusion, we have introduced a model consisting of an optomechanical system directly coupled with a ferromagnetic material. The deformation of the mechanical mode is taken simultaneously due to an optomechanical coupling and the magnetoelasticity of the ferromagnet. We report that the magnetostrictively induced displacement evolves to transfigure the standard OMIT window to Fano profiles in the output field at the probe frequency. The asymmetry of the Fano profiles can be well tuned/controlled by appropriate adjusting the magnon (cavity) detuning and the effective magnomechanical



cal coupling. Remarkably, it is found that the magnetoelastic interaction also gives rise to the FWM phenomenon. FWM intensity can be resonantly tuned by the system's parameters. For example, modulating the effective magnomechanical coupling can realize conversion among a double and triple peak signals. Similarly, in the case of magnon detuning, FWM exhibits the characteristics of symmetric double, triple and even quadruple peak signals. In addition, one can also control the strength of the FWM signals by employing the magnon (cavity) detuning and effective magnomechanical coupling. Moreover, the FWM spectrum exhibits suppressive behavior upon increasing (decreasing) the magnon (cavity) decay. The present OMMS opens new perspectives in highly sensitive detection and quantum information processing, which shall be addressed elsewhere.

### Appendix A. Magnomechanical coupling

The magnetoelastic coupling is fully explained by the interaction between the elastic strain and magnetization of the magnetic material [63, 75]. The magnetoelastic energy density for a cubic crystal is given by [76]

$$F_{me} = \frac{2B_1}{M_s^2} (M_x M_y \epsilon_{xy} + M_x M_z \epsilon_{xz} + M_y M_z \epsilon_{yz}) + \frac{B_2}{M_s^2} (M_x^2 \epsilon_{xx} + M_y^2 \epsilon_{yy} + M_z^2 \epsilon_{zz}), \quad (17)$$

where the magnetoelastic coupling coefficients are represented by  $B_1$  and  $B_2$ .  $M_s$  being the saturation magnetization. In addition, magnetization components are represented by  $M_x$ ,  $M_y$  and  $M_z$ . Furthermore,  $\epsilon_{nm}$  ( $n, m \in x, y, z$ ) defines the strain tensor of the cubic magnetic crystal.

Now, the magnetization can be quantized using the Holstein-Primakoff transformation

$$m = \sqrt{\frac{V}{2\hbar\gamma M_s}} (M_x - iM_y), \quad (18)$$

where  $V$  is the volume of the cubic crystal and  $m$  defines the magnon mode operator. After rearranging, we obtain

$$M_x = \sqrt{\frac{\hbar\gamma M_s}{2V}} (m + m^\dagger), \\ M_y = i\sqrt{\frac{\hbar\gamma M_s}{2V}} (m - m^\dagger), \quad (19)$$

and

$$M_z = [M_s^2 - M_x^2 - M_y^2]^{\frac{1}{2}} \simeq M_s - \frac{\hbar\gamma}{V} m^\dagger m. \quad (20)$$

Putting the value of  $M_{x,y,z}$  in Eq. (17) and then integrating over the volume of the cubic magnetic crystal, the first term in

Eq. (17) yields the semiclassical magnetoelastic Hamiltonian,

$$H_a \simeq \frac{B_1}{M_s} \frac{\hbar\gamma}{V} m^\dagger m \int dl^3 (\epsilon_{xx} + \epsilon_{yy} - 2\epsilon_{zz}) + \frac{B_1}{M_s} \frac{\hbar\gamma}{2V} (m^2 + m^{\dagger 2}) \int dl^3 (\epsilon_{xx} - \epsilon_{yy}) + \frac{B_1}{M_s^2} \frac{\hbar^2 \gamma^2}{V^2} m^\dagger m m^\dagger m \int dl^3 \epsilon_{zz}, \quad (21)$$

and the second term of magnetoelastic energy density from Eq. (17) yields the Hamiltonian

$$H_b \simeq \frac{B_2}{M_s} \frac{\hbar\gamma}{V} (m^2 - m^{\dagger 2}) \int dl^3 \epsilon_{xy} + \frac{2B_2}{M_s} \sqrt{\frac{\hbar\gamma M_s}{2V}} \left[ M_s - \frac{\hbar\gamma}{V} m^\dagger m \right] \times \left[ m \int dl^3 (\epsilon_{xz} + i\epsilon_{yz}) + H.c \right]. \quad (22)$$

Hence, the total magnetoelastic Hamiltonian, which is sum of  $H_a$  and  $H_b$ , implies total magnon-phonon interactions

The magnetoelastic displacement can be defined as:

$$\vec{u}(x, y, z) = \sum_{l,m,n} d^{(l,m,n)} \vec{\chi}^{(l,m,n)}(x, y, z), \quad (23)$$

where  $\vec{\chi}^{(l,m,n)}(x, y, z)$  ( $d^{(l,m,n)}$ ) denotes the normalized displacement eigenmode (the corresponding amplitude).

$$d^{(l,m,n)} = d_{zpm}^{(l,m,n)} (b_{l,m,n} + b_{l,m,n}^\dagger), \quad (24)$$

where  $d_{zpm}^{(l,m,n)}$  represents the amplitude of the zero-point motion. In addition,  $b_{l,m,n}$  and  $b_{l,m,n}^\dagger$  are, respectively the corresponding phononic annihilation and creation operators. Substituting Eqs. (23) and (24) in Eq. (21), the dispersive kind of interaction can be obtained,

$$H_a = \hbar \sum_{l,m,n} g_{mb}^{(l,m,n)} m^\dagger m (b_{l,m,n} + b_{l,m,n}^\dagger), \quad (25)$$

where  $g_{mb}^{(l,m,n)}$  represents the dispersive coupling strength between magnon and phonon, is given by

$$g_{mb}^{(l,m,n)} = \frac{B_1}{M_s} \frac{\gamma}{V} \int dl^3 d_{zmp}^{(l,m,n)} \times \left[ \frac{\partial \chi_x^{(l,m,n)}}{\partial x} + \frac{\partial \chi_y^{(l,m,n)}}{\partial y} - 2 \frac{\partial \chi_z^{(l,m,n)}}{\partial z} \right] \quad (26)$$

In case of a one dimensional mechanical mode oscillation, we obtain the simplified hamiltonian as:

$$H_a = \hbar g_{mb} m^\dagger m (b + b^\dagger), \quad (27)$$

which is the same as the first part of  $H_i$  (see Eq. (3)), since  $q = \frac{1}{\sqrt{2}} (b + b^\dagger)$ . Note that we use the condition of low-lying magnon excitations to derive the above and therefore, the magnon excitation  $m^\dagger m$  second order term (third line of Eq. (21)) can be safely eliminated.

### Data availability

All data used during this study are available within the article.

- 
- [1] M. Aspelmeyer, P. Meystre, and K. Schwab, “Quantum optomechanics”. *Phys. Today* **65**(7) 29 (2012).
- [2] C. H. Dong, V. Fiore, M.C. Kuzyk, and H. L. Wang, “Optomechanical dark mode”. *Science*; **338** 1609 (2012).
- [3] J. K. Moqadam, R. Portugal, M. C. de Oliveira, “Quantum walks on a circle with optomechanical systems”. *Quantum Inf Process* **14**, 3595 (2015).
- [4] J. D. Teufel, T. Donner, M. A. Castellanos-Beltran, J. W. Harlow and K. W. Lehnert, “Nanomechanical motion measured with an imprecision below that at the standard quantum limit”. *Nature nanotechnology* ; **4**(12): 820 (2009).
- [5] A. Motazedifard, A. Dalafi and M. H. Naderi, “Ultraprecision quantum sensing and measurement based on nonlinear hybrid optomechanical systems containing ultracold atoms or atomic Bose-Einstein condensate” *AVS Quantum Sci.* **3**, 024701 (2021)
- [6] Y. Jiao, H. Lu, J. Qian, Y. Li and H. Jing, “Nonlinear optomechanics with gain and loss: amplifying higher-order sideband and group delay”. *New J. Phys.* ; **18**(8):083034 (2016).
- [7] L. M. Ludwig, A. H. Safavi-Naeini, O. Painter and F. Marquardt, “Enhanced quantum nonlinearities in a two-mode optomechanical system”. *Phys. Rev. Lett.* ; **109**(6):063601 (2012).
- [8] S. K. Singh and C. H. Raymond Ooi, “Quantum correlations of quadratic optomechanical oscillator, *J. Opt. Soc. Am. B* **31**, 2390 (2014).
- [9] S. K. Singh and S. V. Muniandy, “Temporal Dynamics and Nonclassical Photon Statistics of Quadratically Coupled Optomechanical Systems”, *Int. J. Theor. Phys.* **55**, 287 (2016).
- [10] A. Sohail, M. Rana, S. Ikram, T. Munir, T. Hussain, R. Ahmed, C. S. Yu. “Enhancement of mechanical entanglement in hybrid optomechanical system”. *Quantum Information Processing* ; **19**(10):372 (2020).
- [11] A. Sohail, *et al.*, “Enhanced entanglement induced by Coulomb interaction in coupled optomechanical systems”. *Phys. Scr.* **95**:035108 (2020).
- [12] S. K. Singh, J. X. Peng, M. Asjad and M. Mazaheri, “Entanglement and coherence in a hybrid Laguerre-Gaussian rotating cavity optomechanical system with two-level atoms”. *J. Phys. B: At. Mol. Opt. Phys.* **54**:215502 (2021).
- [13] Berihu Teklu, Tim Byrnes, Faisal Shah Khan. “Cavity-induced mirror-mirror entanglement in a single-atom Raman laser”. *Phys. Rev. A* **97**:023829 (2018).
- [14] A. Arvanitaki and A. A. Geraci, “Detecting high-frequency gravitational waves with optically levitated sensors”. *Phys. Rev. Lett.* **110**(7):071105 (2013).
- [15] M. S. Ebrahimi, A. Motazedifard, and M. Bagheri Harouni, “Single-quadrature quantum magnetometry in cavity electromagnetics” *Physical Review A* **103** (6), 062605 (2021)
- [16] S. Weis, *et al.* Optomechanically induced transparency. *Science* **330**, 1520 (2010).
- [17] A. H. Safavi-Naeini, *et al.* Electromagnetically induced transparency and slow light with optomechanics. *Nature (London)* **472**, 69 (2011).
- [18] A. Sohail, Y. Zhang, G. Bary, C. S. Yu. “Tunable Optomechanically Induced Transparency and Fano Resonance in Optomechanical System with Levitated Nanosphere”. *IJTP* **57**(9) 2814 (2018).
- [19] A. Sohail, R. Ahmed, C. S. Yu. “Switchable and Enhanced Absorption via Qubit-Mechanical Nonlinear Interaction in a Hybrid Optomechanical System”. *IJTP* **60** 739 (2021).
- [20] F. Monifi, J. Zhang, B. Peng, Yu. Liu, F. Bo, Franco Nori and L. Yang, “Optomechanically induced stochastic resonance and chaos transfer between optical fields”. *Nature Photon.* **10**(6):399 (2016).
- [21] M. Fleischhauer, A. Imamoglu, and J. P. Marangos, “Electromagnetically induced transparency: Optics in coherent media”. *Reviews of modern physics* **77**(2):633 (2005).
- [22] S. K. Singh, M. Parvez, T. Abbas, J. X. Peng, M. Mazaheri, M. Asjad, “Tunable optical response and fast (slow) light in optomechanical system with phonon pump”. *Phys. Lett. A* **442** 128181 (2022).
- [23] S. K. Singh, M. Asjad and C. H. Raymond Ooi, “Tunable optical response in a hybrid quadratic optomechanical system coupled with single semiconductor quantum well”. *Quantum Inf. Process.* **21** 47 (2022).
- [24] A. E. Miroschnichenko, S. Flach, and Y. S. Kivshar, “Fano resonances in nanoscale structures”. *Rev. Mod. Phys.* **82**(3):2257 (2010).
- [25] U. Fano, “Effects of configuration interaction on intensities and phase shifts”. *Phys. Rev.* **124**(6):1866 (1961).
- [26] M. O. Scully, S. Y. Zhu, and A. Gavrielides, “Degenerate quantum-beat laser: Lasing without inversion and inversion without lasing”. *Phys. Rev. Lett.* **62**(24):2813 (1989).
- [27] A. Bärnthaler, S. Rotter, F. Libisch, J. Burgdorfer, S. Gehler, U. Kuhl, and H. J. Stockmann, “Probing decoherence through Fano resonances”. *Phys. Rev. Lett.* **105**(5):056801 (2010).
- [28] M. O. Scully, K. R. Chapin, K. E. Dorfman, M. B. Kim, and A. A. Svidzinsky, “Quantum heat engine power can be increased by noise-induced coherence”. *Proc. Natl. Acad. Sci.* **108**(37): 15097 (2011).
- [29] P. Tassin, L. Zhang, R. Zhao, A. Jain, T. Koschny, and C. M. Soukoulis, “Electromagnetically induced transparency and absorption in metamaterials: the radiating two-oscillator model and its experimental confirmation”. *Phys. Rev. Lett.* **109**(18):187401 (2012).
- [30] Ali Motazedifard, A. Dalafi, M. H. Naderi, “Negative cavity photon spectral function in an optomechanical system with two parametrically-driven mechanical oscillators” *arXiv*:2205.15314 (2022).
- [31] B. Gallinet and O. J. F. Martin, “Ab initio theory of Fano resonances in plasmonic nanostructures and metamaterials”. *Phys. Rev. B* **83**(23):235427 (2011).
- [32] B. Gallinet and O. J. F. Martin, “Influence of electromagnetic interactions on the line shape of plasmonic Fano resonances”. *ACS nano* **5**(11):8999 (2011).
- [33] A. Artar, A. Ali Yanik and H. Altug, “Directional double Fano resonances in plasmonic hetero-oligomers”. *Nano Lett.* **11**(9):3694 (2011).
- [34] S. M. Mozvashi, M. R. Givi, M. B. Tagani, “The effects of sub-

- strate and stacking in bilayer borophene” *Scientific Reports* **12** (1), 1-10 (2022).
- [35] K. Ullah, M. T. Naseem, Ö. E. Müstecaplioglu, “Tunable multi-window magnomechanically induced transparency, Fano resonances, and slow-to-fast light conversion”. *Phys. Rev. A* **102**(3): 033721 (2020).
- [36] A. B. Sabur, A. B. Bhattacharjee. “Magnomechanically induced absorption and switching properties in a dispersively coupled magnon-qubit system”. *J. Appl. Phys.* **132**, 123104 (2022).
- [37] L. Shang, B. Chen, L. L. Xing, J. B. Chen, H. B. Xue, and K. X. Guo, “Controllable four-wave mixing response in a dual-cavity hybrid optomechanical system”. *Chin. Phys. B* **30**(5):295 (2021).
- [38] M. Maeda, “General Remarks: Tunable Sources between Vacuum Ultraviolet and Far Infrared Region”. *Rev. Laser Eng.* **17**(11):744 (1989).
- [39] H. Allahverdi, Ali Motazedifard, A. Dalafi, D. Vitali, and M. H. Naderi, “Homodyne coherent quantum noise cancellation in a hybrid optomechanical force sensor” *Physical Review A* **106** (2), 023107 (2022)
- [40] J. M. Yuan, W. K. Feng, P. Y. Li, Y. Q. Zhang, and Y. P. Zhang, “Controllable vacuum Rabi splitting and optical bistability of multi-wave-mixing signal inside a ring cavity”. *Phys. Rev. A* **86**(6) 063820 (2012).
- [41] H. J. Chen, H. W. Wu, J. Y. Yang, X. C. Li, Y. J. Sun, Y. Peng. “Controllable Optical Bistability and Four-Wave Mixing in a Photonic-Molecule Optomechanics”. *Nanoscale Res. Lett.* **14**(1):73 (2019).
- [42] K. Li, Y. Feng, X. Li, B. Gu, Y. Cai, and Y. Zhang, “Generation of competitive and coexisting two pairs of biphotons in single hot atomic vapor cell”. *Ann. Phys.* **532**(8):2000283 (2020).
- [43] C. Jiang, Y. Cui, H. Liu. “Controllable four-wave mixing based on mechanical vibration in two-mode optomechanical systems”. *EPL (Europhysics Letters)* **104**(3):34004 (2013).
- [44] X. F. Wang, B. Chen. “Four-wave mixing response in a hybrid atom-optomechanical system”. *JOSA B* **36**(2):162 (2019).
- [45] X. Zhang, C. L. Zhang, L. Zou, “Cavity magnomechanics”. *Sci. Adv.* **2** e1501286 (2016).
- [46] F. Heyroth, et al., “Monocrystalline freestanding three-dimensional yttrium-iron-garnet magnon nanoresonators,” *Phys. Rev. Applied.* **12**, 054031 (2019)
- [47] H. Huebl, C. W. Zollitsch, J. Lotze, F. Hocke, A. Marx, R. Gross, and S. T. B. Goennenwein, “High cooperativity in coupled microwave resonator ferrimagnetic insulator hybrids”. *Phys. Rev. Lett.* **111**(12):127003 (2013).
- [48] J. Li, S. Y. Zhu, and G.S. Agarwal, “Squeezed states of magnons and phonons in cavity magnomechanics”. *Phys. Rev. A* **99**(2):021801 (2019).
- [49] D. L. Quirion, Y. Tabuchi, A. Glorpe, K. Usami and Y. Nakamura, “Hybrid quantum systems based on magnonics”. *Appl. Phys. Express* **12**(7):070101 (2019).
- [50] Ali Motazedifard, A. Dalafi and M, H. Naderi, “A Green’s function approach to the linear response of a driven dissipative optomechanical system” *Journal of Physics A: Mathematical and Theoretical* **54** (21), 215301 (2021)
- [51] Xiyun Li, et. al. “Phase control of the transmission in cavity magnomechanical system with magnon driving” *J. Appl. Phys.* **128**, 233101 (2020).
- [52] D. Zhang, X. M. Wang, T. F. Li, X. Q. Luo, W. Wu, F. Nori and J. You, “Cavity quantum electrodynamics with ferromagnetic magnons in a small yttrium-iron-garnet sphere”. *npj Quantum Inf.* **1**(1):15014 (2015).
- [53] C. Gonzalez-Ballester, D. Hummer, J. Gieseler, and O. Romero-Isart, “Theory of quantum acoustomagnonics and acoustomechanics with a micromagnet”. *Phys. Rev. B* **101**(12):125404 (2020).
- [54] C. Kong, B. Wang, Z.-X. Liu, H. Xiong and Y. Wu, “Magnetically controllable slow light based on magnetostrictive forces”. *Opt. express* **27**(4):5544 (2019).
- [55] D. Zhang, X. Q. Luo, Y. P. Wang, T.-F. Li and J.Q. You, “Observation of the exceptional point in cavity magnon-polaritons”. *Nat. commun.* **8**(1):1368 (2017).
- [56] H. Tan, “Genuine photon-magnon-phonon Einstein-Podolsky-Rosen steerable nonlocality in a continuously-monitored cavity magnomechanical system”. *Phys. Rev. Research* **1**(3):033161 (2019).
- [57] M. Asjad, Jie Li, Shi-Yao Zhu and J. Q. You, “Magnon squeezing enhanced ground-state cooling in cavity magnomechanics”. *arXiv* 2022:2203.10767.
- [58] M. S. Ding, L. Zheng and C. Li, “Phonon laser in a cavity magnomechanical system”. *Sci. Rep.* **9**(1):15723 (2019).
- [59] L. Wang, Z. X. Yang, Y. M. Liu, C. H. Bai, D. Y. Wang, S. Zhang and H. F. Wang, “Magnon blockade in a PT-symmetric-like cavity magnomechanical system”. *Ann. Phys.* **532**(7):2000028 (2020).
- [60] C. A. Potts, E. Varga, V. Bittencourt, S. V. Kusminskiy, and J. P. Davis, “Dynamical backaction magnomechanics” *Phys. Rev. X* **11**, 031053 (2021).
- [61] J. Li, S. Y. Zhu, G. S. Agarwal., “Squeezed states of magnons and phonons in cavity magnomechanics”. *Phys. Rev. A* **99**(2):021801 (2019).
- [62] J. Li, S. Y. Zhu, G. S. Agarwal., “Magnon-photon-phonon entanglement in cavity magnomechanics”. *Phys. Rev. Lett.* **121**(20):203601 (2018).
- [63] C. Kittel., “Interaction of spin waves and ultrasonic waves in ferromagnetic crystals”. *Phys. Rev.* **110**(4):836 (1958).
- [64] Z. Y. Fan, R. C. Shen, Y. P. Wang, J. Li, J. Q. You, “Optical sensing of magnons via the magnetoelastic displacement”. *Phys. Rev. A* **105** 033507 (2022).
- [65] X. Zhang, C. L. Zou, L. Jiang, H. X. Tang., “Strongly coupled magnons and cavity microwave photons”. *Phys. Rev. Lett.* **113**(15), 156401 (2014).
- [66] C. Gonzalez-Ballester, D. Hümmer, J. Gieseler, Romero-Isart O. “Theory of quantum acoustomagnonics and acoustomechanics with a micromagnet”. *Phys. Rev. B* **101** (12):125404 (2020).
- [67] C. Genesa, A. Marib, D. Vitali, P. Tombesi., “Quantum Effects in Optomechanical Systems”. **57**:33-86 (2009).
- [68] T. Holstein, H. Primakoff “Field dependence of the intrinsic domain magnetization of a ferromagnet”. *Phys. Rev.* **58**:1098 (1940).
- [69] D. F. Walls, G. J. Milburn, *Quantum Optics* (Springer), Berlin. Heidelberg (1994).
- [70] A. Sohail, Y. Zhang, M. Usman, C. S. Yu, “Controllable optomechanically induced transparency in coupled optomechanical systems”. *Eur. Phys. J. D* **71**(4):103 (2017).
- [71] A. Sohail, R. Ahmed, R. Zainab, C. S. Yu., “Enhanced entanglement and quantum steering of directly and indirectly coupled modes in a magnomechanical system”. *Phys. Scr.* **97075102** (2022)
- [72] A. Sohail, et. al., “Magnon-Phonon-Photon Entanglement via the magnetoelastic Coupling in a Magnomechanical System”. *IJTP* **61**:174 (2022).
- [73] A. Sohail, A. Hassan, R. Ahmed, C. S. Yu., “Generation of enhanced entanglement of directly and indirectly coupled modes in a two-cavity magnomechanical system”. *Quantum Inf. Process.* **21** 207 (2022)
- [74] K. Qu, G. S. Agarwal., “Fano resonances and their control in

- optomechanics". *Phys. Rev. A* **87**(6) 063813 (2013).
- [75] R. Becker and W. Döring, "Ferromagnetismus" Springer, Berlin (1939).
- [76] C. Kittel, "Physical Theory of Ferromagnetic Domains". *Rev. Mod. Phys.* **21** 541 (1949).
- [77] J. W. Rao, et al, "Analogue of dynamic Hall effect in cavity magnon polariton system and coherently controlled logic device, *Nat. Commun.* 10 2934 (2019).
- [78] G. Q. Luo , Z. F. Hu, Y. Liang, L. Y. Yu and L. L. Sun , "Development of low profile cavity backed crossed slot antennas for planar integration" *IEEE Trans. Antennas Propag.* **57** 2972 (2009).